Title:

Outer hair cells stir cochlear fluids

Authors:

Choongheon Lee[1], Mohammad Shokrian[2], Kenneth S. Henry[1, 3, 4], Laurel H. Carney[3, 1, 4], Joseph C. Holt[1, 4, 5], and Jong-Hoon Nam[2, 3, 4] ✉

Author affiliations:

[1] Department of Otolaryngology, University of Rochester, Rochester, NY, United States

[2] Department of Mechanical Engineering, University of Rochester, Rochester, NY, United States

[3] Department of Biomedical Engineering, University of Rochester, Rochester, NY, United States

[4] Department of Neuroscience, University of Rochester, Rochester, NY, United States

[5] Department of Pharmacology and Physiology, University of Rochester, Rochester, NY, United States

Corresponding author:

✉ Email: jong-hoon.nam@rochester.edu

Keywords:

perilymph, kainic acid, outer hair cell, electromotility, organ of Corti, drug delivery

Abstract

Recent observations regarding the non-selective action of outer hair cells contradict frequency-selective cochlear amplification. We hypothesized that active outer hair cells drive cochlear fluid circulation. The hypothesis was tested by delivering a neurotoxin, kainic acid, to the round window of young gerbil cochleae while monitoring auditory responses in the cochlear nucleus. Sounds presented at a modest level significantly expedited kainic acid delivery. When outer-hair-cell motility was suppressed by salicylate, the facilitation effect was compromised. A low-frequency tone was more effective than broadband noise, especially for drug delivery to apical locations. Computational model simulations provided the physical basis for our observation, which incorporated solute diffusion, fluid advection, fluid-structure interaction, and outer-hair-cell motility. Active outer hair cells deformed the organ of Corti like a peristaltic tube to generate apically streaming flows along the tunnel of Corti and basally streaming flows along the scala tympani. Our measurements and simulations coherently indicate that broadband outer-hair-cell action is for cochlear fluid circulation.

Introduction

The inner ear labyrinth is filled with two lymphatic fluids, the perilymph and endolymph. An electrochemical potential difference between the two lymphatic fluids drives hair-cell mechano-transduction (Fettiplace and Kim 2014). Although the inner-ear fluid system is connected to the cerebrospinal fluid of the brain through the cochlear and the vestibular aqueducts and to the vascular system across the blood-labyrinth barrier, inner-ear fluid is virtually isolated from other body-fluid systems (Salt, Thalmann et al. 1986; Ohyama, Salt et al. 1988). Consequently, intervening in hearing health by delivering substances to the inner-ear fluid is challenging. The maintenance of inner-ear fluid composition is achieved locally by the secretion and absorption of ions and molecules through inner-ear epithelial cells (Wangemann and Marcus 2017). As inner-ear fluid homeostasis is maintained locally, a longitudinal electro-chemical gradient exists along the inner-ear labyrinth (Schulte and Schmiedt 1992; Sadanaga and Morimitsu 1995; Hirose and Liberman 2003).

The inner-ear fluid has been reported to be stationary, unlike other lymphatic fluids in the body (Salt and Hirose 2018). Thus, it is considered that substance transport in the inner-ear fluid is governed by diffusion (Salt and Plontke 2005). Diffusion is an effective mechanism for a substance to travel along sub-micrometer distances. For instance, it takes microseconds for neurotransmitters to diffuse across a 20-nm synaptic gap. In contrast, diffusion is inefficient for travel on the centimeter scale. It takes days for a drug applied at the round window to travel 30 mm to the apical end of the human cochlea. In practice, the substance would not reach the apex because it would be resorbed before traveling the distance. Studies on inner-ear drug delivery confirm this principle of physics: Longitudinal mass transport along the inner-ear labyrinth is challenging (Salt, Hartsock et al. 2016; Lukashkin, Sadreev et al. 2020).

The two membranous openings of the inner ear, the oval and round windows, are sites for local delivery of substances into the inner ear. Intratympanic injections of antibiotics and anti-inflammatory drugs have been attempted to manage inner ear disorders despite limited efficacy (Lavigne, Lavigne et al. 2016; Salt and Plontke 2018). Releasing a substance at the end of a long, closed tube forms a steep gradient of concentration. Consequently, the substance does not reach distant regions (Salt and Hirose 2018), whereas, in the vicinity of drug release, the concentration is much higher than desired. One remedy is to inject fluid by making two perforations in the inner ear—one for intruding and the other for extruding (Borkholder, Zhu et al. 2014; Tandon, Kang et al. 2016; Talaei, Schnee et al. 2019). Such an invasive approach requires the injection of a substantial fluid volume, larger than the entire perilymph in the inner ear.

The tube-shaped organ of Corti (OoC) is lined with actuator cells and the cells are activated systematically with a large phase velocity (> a few m/s) toward the apex. A previous study suggests that outer hair cell motility can cause oscillatory fluid motion along the triangular fluid channel within the OoC (Karavitaki and Mountain 2007). Recent measurements of OoC vibrations provide a possible explanation for how this longitudinal fluid flow is generated: outer hair cells operate like an area motor by deforming the OoC cross-sectional area (Jabeen, Holt et al. 2020; Guinan 2022; Lin, Macić et al. 2024). Outer hair cells boost the OoC vibrations over the entire span of the traveling waves (Lee, Raphael et al. 2016; Cooper, Vavakou et al. 2018; He, Kemp et al. 2018; Fallah, Strimbu et al. 2019). In theory, peristaltic deformation of the OoC could induce non-oscillatory streaming along the tunnel of Corti (Shokrian, Knox et al. 2020). This peristaltic motion of the OoC has not been explored experimentally.

78 We hypothesized that outer hair cells agitated by sounds could induce advection of the cochlear fluids.
79 To test this hypothesis, the transport of a neurotoxin along the scala tympani was measured. Kainic acid
80 irreversibly damages the afferent synapses on inner hair cells (Sun, Hashino et al. 2001). Importantly, kainic
81 acid does not affect the hair cells, unlike other popular substances used for inner-ear drug-delivery
82 experiments, such as streptomycin and salicylate (Salt, Hartsock et al. 2016; Lukashkin, Sadreev et al. 2020).
83 Kainic acid (10 mM) was administered at the round-window niche in young gerbils. Multichannel electrodes
84 were inserted into the anteroventral cochlear nucleus (AVCN) to monitor drug effect along the tonotopic
85 axis. The relation between the drug's effect time and location was obtained while controlling sound and
86 activity of outer hair cells, two factors that have not been considered in previous drug-delivery studies. To
87 provide theoretical support for experimental observations, computer models were used to simulate inner-
88 ear drug delivery in three steps: the Virtual Cochlea simulated OoC vibrations due to sound (Zhou and Nam
89 2019); the Navier-Stokes equation including a nonlinear convective term was solved to obtain the drift of
90 the Corti and scala fluids (Shokrian, Knox et al. 2020); and the diffusion-advection equation was solved to
91 simulate the spatiotemporal change of kainic-acid concentration in the cochlear fluids.

92

Results

Outer-hair-cell motility and sound properties, such as frequency, level, and bandwidth, were the parameters that we hypothesized to affect drug delivery. To test the hypothesis, we present a control case and four test cases. The control experiment was the drug delivery in near silence ("Silence"). The test cases included 1) broadband sounds (0.1-12 kHz, 60 or 75 dB SPL) presented during drug delivery ("Sound"), 2) the same broadband sounds presented, but with salicylic acid administered before kainic acid application ("post-SA"), or an 80-dB SPL pure-tone at either 3) 0.5 kHz, ("LF-tone"), or 4) 3-6 kHz ("MF-tone").

Sounds affect inner-ear drug delivery. Before applying 10 mM kainic acid to the round window, the CFs of probing locations were identified (Fig. 1A, D). DPOAEs were measured before and after drug delivery to confirm no change in outer-hair-cell motility during the experiment (Fig. 1C, F). When pre- and post-delivery DPOAEs changed more than 5 dB at any frequency between 0.1 and 10 kHz, the results were excluded (four animals excluded). In one set of experiments, over 90% of stimulus intervals were kept silent (approximately 55 seconds per minute, Fig. 1A-C). In the other experiments, broadband sounds at a modest level (0.1-12 kHz, 60-75 dB SPL) were played during over 90% of the stimulus intervals (Fig. 1D-F). Approximately 8 percent of time (4.6 seconds per minute) were used to acquire background neural activity and to measure responses to 30-40 dB SPL probe tones at three CF frequencies. Under our experimental condition (4 µL of 10-mM kainic acid applied at intact round window), neural responses were abolished after a few to several hundred minutes (Fig. 1B, E). The effect time was defined as the latency following exposure at which the neural response dropped below 75 percent of its baseline value (t_E, Fig. 1B). The drug effect was tonotopic, with higher CF locations being affected earlier (Fig. 1G). In Fig. 1H, the sound- and the silence-case response curves from similar CF locations (between 4.5 and 6.5 kHz) were averaged for comparison. Fig. 1I presents the drug delivery data as the effect time (t_E) versus CF location. We acquired 34 data points from 13 gerbils for the sound protocol and 48 data points from 18 animals for the silence protocol. The trend line (broken curve) was obtained by fitting a curve to the silence-case data points with the 1D diffusion equation (Berg 1983).

To compare the effect times of the sound and silence cases despite varying delivery distances, the effect time was normalized by the trend values at respective CF locations and represented in dB (t_E in dB = $20\log_{10}(t_E/t_{Trend})$, Fig. 1J). Average t_E over the entire CF range was significantly faster for the sound protocol than for the silent case ($p = 0.0045$). Subsequent analyses of low (<4.5 kHz) and mid-frequency (>4.5 kHz) regions further showed that broadband sound exposure increased the speed of drug delivery in the mid-CF region (> 4.5 kHz, $p < 0.001$) but not the low-CF region (< 4.5 kHz, $p = 0.55$; Fig. 1K).

Outer-hair-cell motility was required for the sound effect. Motile outer hair cells boost cochlear responses to sounds. If the sound effect on cochlear drug delivery depends on fluid agitation from outer-hair-cell motility, inhibiting the motility should produce effect times similar to the silent condition. To test this hypothesis, before delivering kainic acid, salicylic acid was administered intraperitoneally (200 mg/kg) to inhibit outer-hair-cell motility. DPOAEs were recorded before and after the salicylic acid application to confirm its effect (Fig. 2A, D). After salicylate injection, neural responses decayed for 20-30 minutes to reach a steady state (Fig. 2B, E). Because the salicylate effect raised the hearing threshold, the probe-tone level was increased by 15-20 dB prior to kainic-acid application (typically from 30 to 50 dB SPL; the discontinuity in the response curve near 70 minutes was due to this increase in the probe tone level). The red-dashed vertical lines of Fig. 2B, E indicate the timing of kainic-acid application. Fig. 2C and F present only the kainic-acid application responses (the time span after the dashed vertical lines in panels B and E).

Note that 75-dB SPL broadband sounds were played in the post-SA protocol. The two examples in Fig. 2A-F also demonstrate the variance of the salicylate effect. In one case, DPOAEs decreased by < 10 dB (re: 40 dB stimulation) and the neural responses to 30 dB SPL sound decreased by 40 percent (Fig. 2B). In the other case, DPOAEs decreased by approximately 20 dB, and the neural responses to 30 dB SPL sound decreased to the noise floor. For the post-SA protocol, we acquired 24 data points from 8 animals. The post-kainate response decay of salicylate-treated ears followed the trend of the silence case despite use of the sound protocol (Fig. 2G). Despite the sound stimulation, the effect time of the post-SA case was not different from the silence case ($p = 0.096$) and was greater than the sound case ($p < 0.001$, Fig. 2I). Like the silence versus sound protocols comparison, the statistical difference was from the mid-CF locations, not from low-CF locations (Fig. 2I). The post-SA results support the hypothesis that outer-hair-cell motility is required for faster inner-ear drug delivery with sound exposure.

Low-frequency tones were more effective. If the sound effect on cochlear drug delivery were due to fluid agitation, other sounds might be more effective than random noise. Vibrations along the cochlear partition propagate with decaying phase velocity toward the apex, before stalling shortly after reaching the sound's CF location. Advective flow of the cochlear fluid is shaped by the vibration frequency and amplitude and by the phase velocity of traveling waves (Lighthill, 1993; Shokrian, Nam, 2020). To test the hypothesis that the type of sound stimulus varied the effectiveness of drug delivery, especially in low-frequency regions, pure-tones at 80 dB SPL were played during inner-ear drug delivery, instead of broadband noise. In choosing the frequency of pure tone, we considered the nature of cochlear traveling waves, guided by fluid-dynamics simulations (Zhou and Nam 2019; Shokrian, Knox et al. 2020). The frequency of 0.5 kHz was chosen close to the low bound of the gerbil's audible frequency range. The mid-frequency was selected from between 3 and 6 kHz to match the CF location of one of the electrode probes. If the sound facilitation were most prominent near the peak of traveling waves, the low-frequency tone would be inefficient in facilitating drug delivery to high- to mid-CF locations. Whereas, if the phase velocity were crucial for fluid agitation, the low-frequency sound should be advantageous because of its long tail region with high phase velocity. If the traveling wave pattern set the cochlear fluid flow, the sound-facilitation effect could stall at one location, similar to the traveling waves.

With the pure-tone protocol, 45 data points were acquired from 15 gerbils. In two example cases, the effect time at low-CF locations (CFs near 2 kHz) was 15 minutes for the case of the 0.5 kHz tone (Fig. 3A) and 100 minutes for the 3.5 kHz tone (Fig. 3B). In the mid-CF locations, the effect time did not differ for different tone frequencies: the effect time ranged between 8 and 12 minutes for CF locations between 5.9 and 6.3 kHz (red curves of Fig. 3A, B). In some cases, especially toward the low-CF locations, the response curve had bimodal decay patterns (e.g., the cyan curve in Fig. 3B), resulting in a broader distribution in the effect time. The overall plots of effect time versus location (Fig. 3C, D) show that most data points are below the trend line of the control (silence) case. That is, the pure-tone stimulation facilitated the delivery throughout the cochlea. According to the statistical analysis of effect time differences between the silence and the pure-tone protocols (Fig 3E), low-frequency tones facilitated the drug delivery for both low- ($p < 0.001$) and mid-CF locations ($p = 0.011$). Mid-frequency tones facilitated for mid-CF locations ($p < 0.001$) but not significantly for low-CF locations ($p = 0.084$). Low-frequency tones were more effective than broadband noise especially at the apical low-CF locations (Fig. 3F, $p < 0.0005$ for all CF locations, $p < 0.00001$ for apical locations with CF < 4.5 kHz).

Figure 4 summarizes our findings for all four cases—control (delivery in silence, Fig. 4A, B), sound (broadband noise at 60 or 75 dB SPL, Fig. 4C, D), post-SA sound (SA applied IP or to the round window 30-40

min before kainic-acid application, broadband noise at 75 dB SPL, Fig. 4E, F), and pure-tone sound (either 0.5 kHz or 3-6 kHz at 80 dB SPL, Fig. G, H). The broken trend lines shown in all panels are the same, obtained by a curve fit to the control (silence) data using the 1D diffusion equation. Broadband sounds decreased the effect time in the mid-CF locations (CF > 4.5 kHz) but had little effect in the low-CF locations (CF < 4.5 kHz, Fig. 4C, D). While measurements at two levels (60 and 75 dB SPL) were pooled in Fig. 1, they are distinguished in Fig. 4C and D. Although the mean effect time of the 75 dB SPL data was smaller than for 60 dB SPL in the mid-CF region, supporting the sound-facilitation hypothesis, a larger sample number will be required to confirm the effect of sound level. The sound effect disappeared after inhibiting outer-hair-cell motility with salicylate (Fig. 4E, F). In Fig. 2, only IP-administered data of the post-SA case are presented. Fig. 4E and F include additional data on the local (round-window) application of salicylate before applying a solution containing 10 mM kainic acid and 100 mM salicylic acid. While the local-delivery case reduced the mean effect time in the mid-CF region, the effect times of both post-SA cases were not significantly different from the control case. For the mid-CF region, the difference in mean effect time between the two post-SA cases was ascribed to the incomplete inhibition of outer hair cells in the local-delivery case. The most prominent effect was observed when the drug was delivered while playing a low-frequency tone. For instance, 17 out of 18 effect times for the LF-tone case (red square symbols, Fig. 4G and H) were below the trend line of the control (silence) case.

The mechanism of sound facilitation for drug delivery was investigated with computer model simulations. Our computer model is distinguished from most cochlear mechanics models in three aspects. First, it incorporates the interactions between the Corti fluid and OoC structures. Second, the nonlinear advection term in the Navier-Stokes equation was not neglected. Finally, both diffusion and fluid advection were considered. Our simulated results support the hypothesis that the cross-sectional area change of the OoC performs like a peristaltic pump (i.e., active outer hair cells are the fluid pumps) (Shokrian, Knox et al. 2020). Fig. 5 shows half of the cochlear fluid space—the scala tympani and the OoC fluid spaces (omitting the scala media and scala vestibuli). We simulated two cases: In the silence case, the drug delivery was purely governed by diffusion (Fig. 5A). In the LF-tone case, both diffusive and advective mass transports contributed (Fig. 5B-D). For the LF-tone case, a 1-kHz tone at 80 dB SPL sound was played continuously. The contours in Fig. 5A and B represent the concentration of the substance at 30 minutes after the onset of delivery. As expected from Fick's law and the log-scale plots of Fig. 4, the gradient over distance decays logarithmically. That is, contour lines in Fig. 5A have similar spacings in the log scale. However, such a logarithmic gradient was apparently disturbed between the 0.1 and 0.01 mM contour lines in Fig. 5B. The contour line is stretched toward the right (red double-headed arrow) in the top Corti fluid layer and to the left (blue arrow) in the bottom scala fluid layer. This stretched contour line was due to the advective flow. In Fig. 5C and D, the contour lines represent the streamlines (i.e., particles would drift along the contour lines). The red and blue colors indicate clockwise and counterclockwise circulation, respectively. Fig. 5D presents the fluid streaming near the peak of the traveling wave (6-9.5 mm from the base, Corti fluid and top 120 µm-thick scala fluid). The maximum streaming velocity is as substantial as a few mm/s. Our simulation shows that active outer hair cells generate a strong stream toward the apex along the tunnel of Corti. The displaced fluid in the apex flows toward the base along the bottom of the scala tympani. The strong advection takes place in the tail of the traveling wave, over a few mm.

Discussion

We showed that sound exposure increases drug delivery from the round window to mid-frequency and apical cochlear locations. Sound-facilitated drug delivery was compromised when outer-hair-cell motility was inhibited. Low-frequency tones were more effective than broadband noise in delivering substances to the apex of the cochlea. These results not only highlight new strategies for improving drug delivery throughout the cochlear spiral, but reveal a new function of outer hair cells, beyond sound amplification.

Neural responses near CF are amplified, showing enhanced tuning. In contrast, outer hair cells boost the vibrations in the OoC non-selectively (Cooper, Vavakou et al. 2018; He, Kemp et al. 2018; Fallah, Strimbu et al. 2019). To reconcile the nonselective input (untuned OoC vibrations) and the selective output (tuned neural signals), previous studies suggest that outer hair cells accumulate their power along cochlear traveling waves, referred to as global amplification (Zagadou and Mountain 2012; He, Burwood et al. 2022). However, experimental evidence is incongruent with the global amplification theory (Fisher, Nin et al. 2012; Versteegh and van der Heijden 2013; Dewey, Applegate et al. 2019). According to the two-tone suppression experiment of Dewey et al. (2019), the suppression of outer hair cells far basal from the CF location does not affect the response at the CF location. Available evidence shows that the amplification due to outer-hair-cell action occurs between a location one half-octave basal to the peak and the peak location (Dong and Olson 2013; Fallah, Strimbu et al. 2019). The present study provides new insights into the nonselective outer hair cell action.

Broadband action of outer hair cells helps cochlear-fluid circulation. Our pure-tone experiments (Fig. 3) and simulation (Fig. 5) show that the region of sound-facilitated drug delivery spanned regions far basal to the CF location of a given sound frequency. Such sound facilitation disappeared when outer hair cell motility was suppressed (Figs. 2), which implied that active outer hair cells are the stirrers in the cochlea that drive lymphatic-fluid circulation. From an evolutionary perspective, mammals stretched their hearing organ to encode broader bandwidth with good frequency resolution. The longer cochlea might have entailed a challenge: Maintaining the freshness of the stationary lymph along a long and narrow tube is nontrivial. For instance, a local failure in homeostasis could cascade along the cochlea, making the system vulnerable to disturbance or trauma. The OoC in the basal cochlea suffers from a maintenance burden: a greater influx of potassium (greater MET current) and a smaller clearance surface. We hypothesize that the longitudinal circulation of lymphatic fluid serves as a protective mechanism for the fluid homeostasis of the mammalian cochlea.

The nature of the streaming pattern supports the feasibility of targeted inner-ear drug delivery. Two characteristics implicated in the pure-tone experiments (Fig. 3) became apparent in the model simulations (Fig. 5): the advection caused by active outer hair cells created a ‘fast track’ and a ‘stalling point’ for mass transport. For instance, the span between locations 5.5 and 9 mm is the fast track of mass transport (the arrows of concentration contours in Fig. 5B and the clockwise advective flow in Fig. 5C). In this fast track, the distance between contour lines is much larger than the other regions or the pure diffusion case. The contour line in the fast track (black curve, Fig. 5B) is stretched toward the apex in and near the Corti fluid and toward the base at the bottom of the scala tympani, indicating longitudinal fluid circulation. In contrast to the fast track region, there was a stalling point where the transport stopped. The stacking contours near 10 mm in Fig. 5B are caused by the countering circulation loops at 9 mm in Fig. 5C. Taking advantage of

these ‘fast tracks’ and ‘stalling points’, one could design a sequence of sounds to deliver a substance from the round window to a targeted location in the cochlea.

261 ## Materials and Methods

262 **Experimental approach**

263 **Animal Preparation:** Sixty-four Mongolian gerbils (*Meriones unguiculatus,* 25 males and 39 females,
264 Charles River Laboratories) were 2-3 months of age. All experimental procedures were in accordance with
265 NIH guidelines and approved by the University of Rochester Animal Care and Use Committee. Animals were
266 anesthetized with an intraperitoneal injection of ketamine (140 mg/kg) and xylazine (6 mg/kg) and placed
267 on a closed-loop heating pad to maintain body temperature at 37 ± 0.5 °C. Ketamine and xylazine were
268 then administered continuously through a subcutaneous catheter at a baseline rate of 85 and 3.5 mg/kg/hr,
269 respectively, and adjusted as needed to maintain an areflexic state. Supplemental intraperitoneal injections
270 of ketamine and xylazine were occasionally administered as required. A tracheotomy and intubation
271 ensured an open airway. Breathing rate was monitored using a thermistor placed in front of the trach tube.
272 The right pinna was removed, and the bulla was exposed. A hole made in the dorsal and caudal bulla
273 allowed access to the temporal bone and round window. After securing the skull using dental acrylic,
274 customized headpost and ear bars, and a stereotaxic frame (Kopf Instruments, Model 900), a craniotomy
275 was made in the temporal bone for electrode penetration through the dura to the AVCN. The head was
276 oriented with the nose pitching downward at 45 degrees so that the round window niche faced upward to
277 better contain the pharmaceutical solution.

278 **Drugs used:** Pharmacological agents included the kainic receptor agonist kainic acid (Abcam and
279 Tocris) and sodium salicylate (Sigma-Aldrich). A 10 mM kainic acid solution (volume of 4 µL) was applied at
280 the round window niche. The kainic acid solution was prepared in Hank's balanced salt solution (HBSS,
281 Sigma-Aldrich). No discernible effects of different solvents on the AVCN responses were observed (data not
282 shown). Sodium salicylate was dissolved in HBSS for local round-window delivery at a concentration of 100
283 mM (volume of 4 µL) or dissolved in saline for intraperitoneal injection at a dose of 200 mg/kg (volume of
284 0.3 mL).

285 **Measurement protocol**: All experiments were performed in a soundproof chamber. A pair of speakers
286 and a microphone (ER-2 and ER-10, Etymotic) were plugged and sealed into the ear canals through a
287 coupler. The sound pressure level (SPL) in the ear canal was calibrated between 0.1 and 16 kHz. A reference
288 electrode was inserted into the muscles of the back of the neck. A multi-channel electrode (Q1x4-10mm-
289 100-177-EIB, Neuronexus or ASSY-37 Fb Acute 32 channel, Cambridge Neurotech) was advanced 2-3-mm
290 into the AVCN using a hydraulic microdrive (Model 640, Kopf Instruments), with a rostro-caudal angle
291 between 60-65 degrees and lateral angle between 40-50 degrees with respect to the interaural line. The
292 characteristic frequencies (CFs) of the four multi-unit channels were identified using tones. . Typically, three
293 channels were identified showing well defined frequency tuning and distinct CFs (Fig. 1A, D). Neural
294 responses were amplified and bandpass filtered between 0.75-10 kHz, then sampled (National Instruments
295 PCIe-6251, 50 kHz or Intan RHD 2000, 30 kHz) for storage on a computer hard drive. Neural recordings were
296 transformed with a Teager energy operator to enhance spiking activity (Choi et al., 2006) and the average
297 value of the Teager-transformed response waveform was taken as a measure of the neural response
298 amplitude. Typical time courses of neural signals are shown in Fig. 1C and F (kainic acid was administered at
299 t = 0). Experiments lasted between 1 and 3 hours.

300

301 Drug solutions were applied either at the round window niche using a 100 µL Hamilton syringe or
302 through intraperitoneal injection. After experiments, it was confirmed that the solution was still contained

303 in the round window niche. While kainic acid diffused into the cochlea, the neural signals from the AVCN
304 were recorded under three acoustical conditions: For the "Sound" protocol, 1.1-s noise pips (60 or 75 dB
305 SPL, 0.1-12 kHz bandwidth, 0.8-s duration including 0.15-s onset/offset ramps) were presented
306 continuously. After 48 noise pips, one 1.1-s silent pause and three CF tone pips followed (a total of 51 pips
307 and a pause make a 57.2-s pack). The CF tone pips were presented at the level of 35 dB SPL to monitor
308 neural responses. The silence pause was to monitor spontaneous neural responses. The pack was repeated
309 until neural signals at the lowest probing CF were completely abolished. The neural responses presented in
310 this study are the 'driven responses' obtained by subtracting the spontaneous responses from the
311 responses at the 35 dB CF tones. For the "Silence" or "Pure-tone" protocol, the noise pips of the Sound
312 protocol were replaced with either silence pauses or a pure tone at 80 dB SPL. The pure tone frequency was
313 either 0.5 kHz or a frequency between 3 and 6 kHz matching one of the mid-frequency probe channels.
314 Stimuli were generated in Matlab (50-kHz sampling frequency), converted to analog (National Instruments
315 PCIe-6251), adjusted to the desired level using analog attenuation (PA5; Tucker Davis Technologies,
316 Alachua, FL), and presented using a headphone buffer amplifier (HB7; Tucker Davis Technologies).

317 **Distortion product otoacoustic emissions (DPOAEs)**: DPOAEs before and after the kainic acid delivery
318 measurement were used to confirm that outer hair cell function did not change (Fig. 1C, F). DPOAEs were
319 recorded in response to swept primary tones, f_1 and f_2, with f_2 increasing linearly from 0.5 to 10 kHz over 4
320 seconds, and $f_2 = 1.25\ f_1$. Primary tones (4.05-s duration including 25-ms raised-cosine on/off ramps, with
321 300-ms inter-stimulus intervals) were presented from separate earphones with equal sound levels, from
322 40-70 dB in 10-dB steps. DPOAEs were amplified by 40 dB prior to sampling and were averaged across 10
323 stimulus presentations. DPOAE level at $2f_1$- f_2 was estimated using a least-squares fitting procedure (Long et
324 al., 2008) in Matlab, based on a 100-ms Hann window shifted in 20-ms steps (Wong et al., 2019). The same
325 analysis was applied to a 'null' response, computed as the difference between average even and odd-
326 numbered stimulus presentations, to determine the noise floor.

327 **Modeling approach**

328 Cochlear fluid dynamics were divided into three sequential stages. Different assumptions were used in
329 each stage to represent the relevant physics appropriately and to make the computational analyses
330 affordable. First, OoC vibration due to sound stimulation was estimated by solving fluid-structure
331 interactions between scala fluids, the Corti fluid (extracellular fluid in the OoC) and the OoC. The active
332 feedback from outer-hair-cell motility was incorporated into OoC mechanics. Second, the drift velocity of
333 the fluids in the OoC and the scala tympani in response to OoC vibrations was computed. Drift velocity
334 originates from the nonlinear convective term in the governing equations for the incompressible flow (ref
335 Shokrian et al 2020). The spatial resolution required to evaluate the drift velocity made this stage
336 computationally costly. Unlike the first stage, the advective component of fluid motion was incorporated.
337 The OoC vibrations obtained at the first stage were given as kinematic boundary conditions in this second
338 stage. The fluid motion within the OoC, as well as in the scala tympani, was computed. Third, the
339 spatiotemporal pattern of substance concentration due to advection and diffusion was obtained. The drift
340 velocity field obtained in the second stage was the input for this third stage. The first and second stages
341 were simulated using custom-written Matlab programs, while the third stage was solved using
342 commercially available software (COMSOL multiphysics).

343 **OoC vibrations**: The OoC complex structures were discretized into 3-D finite elements reflecting
344 anatomical details. For instance, each hair bundle, hair cell, Deiters cell, or pillar cell was represented by a
345 fully deformable beam. The tectorial and basilar membranes were presented by a meshwork of beams.

346 Their mechanical properties were determined either by using known values or by comparing them with
347 existing mechanical measurements (Nam and Fettiplace 2010; Liu, Gracewski et al. 2017; Marnell, Jabeen et
348 al. 2018). Mechano-transduction kinetics of hair bundle and outer-hair-cell electromotility were
349 incorporated with the OoC finite-element model (Nam and Fettiplace 2012; Nam 2014). The scala-fluid
350 domain was discretized into linear quadrilateral elements. The scala-fluid pressure was determined by two
351 vibrating boundaries—one is the oval window, and the other is the OoC complex. In turn, the OoC
352 structures vibrate due to differential pressure across the OoC.

353 **Drift velocity of fluids**: From the round window to the inner hair cell, kainic acid molecules travel
354 (drift) across two fluid spaces separated by the basilar membrane: 1) the Corti fluid, and 2) the scala-
355 tympani fluid. The Corti fluid includes the fluid in the tunnel of Corti, Nuel's space, gaps between outer hair
356 cells, and the outer tunnel. These sub-spaces are interconnected to one another by a few micrometer gaps.
357 For simplicity, the 3-D fluid spaces were reduced to 2-D after reducing the radial dimension. The top
358 boundary of the 2-D Corti fluid was modeled as a deforming wall while the bottom surface shared with
359 scala tympani was implemented as a permeable boundary representing the basilar membrane. The OoC
360 deformation was represented by the relative motion between the top and bottom surfaces of the Corti
361 fluid. The pressure (p) and velocity ($\mathbf{u}$) of the incompressible fluid were determined by the Navier-Stokes
362 and continuity equations.

$$\frac{\partial \mathbf{u}}{\partial t} + \mathbf{u} \cdot \nabla \mathbf{u} = -\frac{1}{\rho}\nabla p + \nu \nabla^2 \mathbf{u}, \text{ and} \tag{1}$$

$$\nabla \cdot \mathbf{u} = 0, \tag{2}$$

363 where ν and ρ are the kinematic viscosity (70×10^{-6} m^2/s) and density (1 g/cm^3). Note that this viscosity
364 value is a hundred times the value of the water after Prodanovic et al. (2019). The second term in Eq 1
365 representing advection renders this equation nonlinear. This term has been neglected in cochlear
366 mechanics studies because it hardly contributes to forming the cochlear traveling waves. However, for the
367 purpose of this work (to investigate cochlear mass transport due to advection), this term had to be
368 incorporated despite the increased computational cost. The basilar membrane was considered to have
369 finite permeability using Darcy's law. The fluid velocity passing through the basilar membrane (u_p) is
370 proportional to the transmembrane pressure difference Δp), or

$$u_p = -K\Delta p. \tag{3}$$

371 The value of the permeability coefficient, K, of 1 $\mathrm{m/(sPa)}$ was empirically determined so that the
372 Corti-fluid pressure level was not excessive (< a few Pa). Preliminary simulation results showed that drift
373 velocities were not sensitive to the chosen value of K, even over an order of magnitude from the chosen
374 value. Because of the basilar membrane's permeability, in general, the fluid velocity just above or below
375 the basilar membrane (u_f) is different from the basilar membrane velocity (u_m) by u_p, or

$$u_f = u_m + u_p. \tag{4}$$

376 When periodic stimulation was applied, the resulting fluid motion was also periodic. Albeit much
377 smaller than oscillatory motion, there existed non-periodic fluid motion that made fluid particles drift over
378 time. When fluid motion is integrated over a period, T, the oscillatory component cancels out, leaving only
379 drift. The drift velocity $\mathbf{u}_D$ at position $\mathbf{x}_p$ and time $t + 0.5T$ was computed as

$$\mathbf{u}_D(\mathbf{x}_p, t + 0.5T) = \frac{1}{T}\int_t^{t+T} \mathbf{u}_\mathrm{E}(\mathbf{x}_p, \tau) d\tau, \tag{5}$$

where $\mathbf{u}_\mathrm{E}$ is the Eulerian velocity obtained as a solution of the Navier-Stokes equations.

Diffusion: Mass transport is governed by the advection-diffusion equation.

$$\frac{\partial C}{\partial t} = D\,\nabla^2 C - \mathbf{u}_D \cdot \nabla C, \tag{6}$$

where C is the concentration of the transported substance and D is the diffusion coefficient. The whole fluid domain is impermeable (or $\partial C/\partial n = 0$, n is the vector normal to the surface) except for the round window and the basilar membrane. At the round window, the concentration level was constant at 10 mM. The effect time at a specific location was defined as the time to reach 1% of the round-window concentration (100 µM).

Computation: The mesh for the fluid dynamics model (the first stage, Eqs. 1 and 2) consisted of approximately 25,000 second-order quadrilateral elements with the same degrees of freedom for both velocity and pressure. The grid size of the mesh was determined considering the boundary layer thickness of $(\nu/\omega)^{0.5}$, where ω was the highest frequency component of stimulation. The time integration was carried out using the second-order Crank-Nicolson method. The least-squares finite element approach was used with a reduced-order integration to ensure stability. The time-step size was 10 µs, and the problem was solved in the time domain for 5 ms (sufficient time to reach a periodical steady state). This time length was long enough to arrive at the periodic steady state. The mesh resolution for diffusion analysis was approximately 1 µm, resulting in about 225,000 first-order triangular elements. The initial time step was equal to the period of the stimulating frequency (1 ms) and was increased adaptively based on the convergence rate.

Data and codes availability: The data used in this study will be made available through a publicly accessible repository when accepted. The following temporary link contains the source codes to simulate Fig. 5. https://figshare.com/s/600fc65f56587d473d48 When published, this private link will become public.

Funding

National Institute of Health NIDCD R01 DC020150 (PI: J-H Nam)
The funder had no role in study design, data collection and interpretation, or the decision to submit the work for publication.

Acknowledgements

The authors thank Jonathan Becker and Kris Abrams for their technical assistances.

Author contributions

CL, MS, and KSH contributed to this work equally. JHN, KSH, and LHC conceived and designed experimental part of the study. JHN and MS conceived and designed computational part of the study. KSH and CHL were the primary experimentalists who acquired experimental data. JHN, LHC and JCH participated in experiments. KHS wrote the codes to acquire data. JHN, KSH, LHC, and CHL analyzed experimental data. MS was the primary computational modeler. MS and JHN developed the computational analysis codes. MS simulated the computational codes. JHN drafted the MS and created the figures. JHN, MS, KSH, LHC, and JCH wrote the paper together.

Author ORCIDs

Jong-Hoon Nam https://orcid.org/0000-0002-7477-5453
Kenneth S. Henry https://orcid.org/0000-0003-1364-318X
Laurel H. Carney https://orcid.org/0000-0002-4729-5702

Joseph C. Holt https://orcid.org/0000-0001-7908-083X

Ethics

All experimental procedures were in accordance with NIH guidelines and approved by the University of Rochester Animal Care and Use Committee (protocol #: 101066).

429 ## References

430 Berg, H. C. (1983). Random walks in biology. Princeton, N.J., Princeton University Press.
431 Borkholder, D. A., X. Zhu and R. D. Frisina (2014). "Round window membrane intracochlear drug delivery
432 enhanced by induced advection." J Control Release **174**: 171-176.
433 Cooper, N. P., A. Vavakou and M. van der Heijden (2018). "Vibration hotspots reveal longitudinal funneling
434 of sound-evoked motion in the mammalian cochlea." Nat Commun **9**(1): 3054.
435 Dewey, J. B., B. E. Applegate and J. S. Oghalai (2019). "Amplification and Suppression of Traveling Waves
436 along the Mouse Organ of Corti: Evidence for Spatial Variation in the Longitudinal Coupling of Outer Hair
437 Cell-Generated Forces." J Neurosci **39**(10): 1805-1816.
438 Dong, W. and E. S. Olson (2013). "Detection of cochlear amplification and its activation." Biophys J **105**(4):
439 1067-1078.
440 Fallah, E., C. E. Strimbu and E. S. Olson (2019). "Nonlinearity and amplification in cochlear responses to
441 single and multi-tone stimuli." Hear Res **377**: 271-281.
442 Fettiplace, R. and K. X. Kim (2014). "The physiology of mechanoelectrical transduction channels in hearing."
443 Physiol Rev **94**(3): 951-986.
444 Fisher, J. A., F. Nin, T. Reichenbach, R. C. Uthaiah and A. J. Hudspeth (2012). "The spatial pattern of cochlear
445 amplification." Neuron **76**(5): 989-997.
446 Guinan, J. J. (2022). "Cochlear amplification in the short-wave region by outer hair cells changing organ-of-
447 Corti area to amplify the fluid traveling wave." Hearing Research **426**.
448 He, W., G. Burwood, E. V. Porsov, A. Fridberger, A. L. Nuttall and T. Ren (2022). "The reticular lamina and
449 basilar membrane vibrations in the transverse direction in the basal turn of the living gerbil cochlea." Sci
450 Rep **12**(1): 19810.
451 He, W., D. Kemp and T. Ren (2018). "Timing of the reticular lamina and basilar membrane vibration in living
452 gerbil cochleae." Elife **7**.
453 Hirose, K. and M. C. Liberman (2003). "Lateral wall histopathology and endocochlear potential in the noise-
454 damaged mouse cochlea." J Assoc Res Otolaryngol **4**(3): 339-352.
455 Jabeen, T., J. C. Holt, J. Becker and J. H. Nam (2020). "Interactions between passive and active vibrations in
456 the organ of Corti In vitro." Biophysical Journal **119**(2): 314-325.
457 Karavitaki, K. D. and D. C. Mountain (2007). "Evidence for outer hair cell driven oscillatory fluid flow in the
458 tunnel of corti." Biophys J **92**(9): 3284-3293.
459 Lavigne, P., F. Lavigne and I. Saliba (2016). "Intratympanic corticosteroids injections: a systematic review of
460 literature." Eur Arch Otorhinolaryngol **273**(9): 2271-2278.
461 Lee, H. Y., P. D. Raphael, A. Xia, J. Kim, N. Grillet, B. E. Applegate, A. K. Ellerbee Bowden and J. S. Oghalai
462 (2016). "Two-Dimensional Cochlear Micromechanics Measured In Vivo Demonstrate Radial Tuning within
463 the Mouse Organ of Corti." J Neurosci **36**(31): 8160-8173.
464 Lin, W.-C., A. Macić, J. Becker and J. H. Nam (2024). "Asymmetric vibrations in the organ of Corti by outer
465 hair cells measured from excised gerbil cochlea." Commun Biol(In press).
466 Liu, Y., S. M. Gracewski and J. H. Nam (2017). "Two passive mechanical conditions modulate power
467 generation by the outer hair cells." PLoS Comput Biol **13**(9): e1005701.
468 Lukashkin, A. N., Sadreev, II, N. Zakharova, I. J. Russell and Y. M. Yarin (2020). "Local Drug Delivery to the
469 Entire Cochlea without Breaching Its Boundaries." iScience **23**(3): 100945.
470 Marnell, D., T. Jabeen and J. H. Nam (2018). "Hydrostatic measurement and finite element simulation of the
471 compliance of the organ of Corti complex." J Acoust Soc Am **143**(2): 735.
472 Nam, J. H. (2014). "Microstructures in the organ of Corti help outer hair cells form traveling waves along the
473 cochlear coil." Biophys J **106**(11): 2426-2433.
474 Nam, J. H. and R. Fettiplace (2010). "Force transmission in the organ of Corti micromachine." Biophys J
475 **98**(12): 2813-2821.

476 Nam, J. H. and R. Fettiplace (2012). "Optimal electrical properties of outer hair cells ensure cochlear
477 amplification." PLoS One **7**(11): e50572.
478 Ohyama, K., A. N. Salt and R. Thalmann (1988). "Volume flow rate of perilymph in the guinea-pig cochlea."
479 Hear Res **35**(2-3): 119-129.
480 Prodanovic, S., S. M. Gracewski and J. H. Nam (2019). "Power Dissipation in the Cochlea Can Enhance
481 Frequency Selectivity." Biophys J **116**(7): 1362-1375.
482 Sadanaga, M. and T. Morimitsu (1995). "Development of endocochlear potential and its negative
483 component in mouse cochlea." Hear Res **89**(1-2): 155-161.
484 Salt, A. N., J. J. Hartsock, R. M. Gill, E. King, F. B. Kraus and S. K. Plontke (2016). "Perilymph
485 pharmacokinetics of locally-applied gentamicin in the guinea pig." Hear Res **342**: 101-111.
486 Salt, A. N. and K. Hirose (2018). "Communication pathways to and from the inner ear and their
487 contributions to drug delivery." Hear Res **362**: 25-37.
488 Salt, A. N. and S. K. Plontke (2005). "Local inner-ear drug delivery and pharmacokinetics." Drug Discov
489 Today **10**(19): 1299-1306.
490 Salt, A. N. and S. K. Plontke (2018). "Pharmacokinetic principles in the inner ear: Influence of drug
491 properties on intratympanic applications." Hear Res **368**: 28-40.
492 Salt, A. N., R. Thalmann, D. C. Marcus and B. A. Bohne (1986). "Direct measurement of longitudinal
493 endolymph flow rate in the guinea pig cochlea." Hear Res **23**(2): 141-151.
494 Schulte, B. A. and R. A. Schmiedt (1992). "Lateral wall Na,K-ATPase and endocochlear potentials decline
495 with age in quiet-reared gerbils." Hear Res **61**(1-2): 35-46.
496 Shokrian, M., C. Knox, D. H. Kelley and J. H. Nam (2020). "Mechanically facilitated micro-fluid mixing in the
497 organ of Corti." Sci Rep **10**(1): 14847.
498 Sun, H., E. Hashino, D. L. Ding and R. J. Salvi (2001). "Reversible and irreversible damage to cochlear
499 afferent neurons by kainic acid excitotoxicity." J Comp Neurol **430**(2): 172-181.
500 Talaei, S., M. E. Schnee, K. A. Aaron and A. J. Ricci (2019). "Dye Tracking Following Posterior Semicircular
501 Canal or Round Window Membrane Injections Suggests a Role for the Cochlea Aqueduct in Modulating
502 Distribution." Front Cell Neurosci **13**: 471.
503 Tandon, V., W. S. Kang, T. A. Robbins, A. J. Spencer, E. S. Kim, M. J. McKenna, S. G. Kujawa, J. Fiering, E. E.
504 Pararas, M. J. Mescher, W. F. Sewell and J. T. Borenstein (2016). "Microfabricated reciprocating micropump
505 for intracochlear drug delivery with integrated drug/fluid storage and electronically controlled dosing." Lab
506 Chip **16**(5): 829-846.
507 Versteegh, C. P. and M. van der Heijden (2013). "The spatial buildup of compression and suppression in the
508 mammalian cochlea." J Assoc Res Otolaryngol **14**(4): 523-545.
509 Wangemann, P. and D. C. Marcus (2017). Ion and fluid homeostasis in the cochlea. Understanding the
510 Cochlea. G. A. Manley and A. W. Gummer, Springer, Cham. **62:** 253-286.
511 Zagadou, B. F. and D. C. Mountain (2012). "Analysis of the cochlear amplifier fluid pump hypothesis." J
512 Assoc Res Otolaryngol **13**(2): 185-197.
513 Zhou, W. and J. H. Nam (2019). "Probing hair cell's mechano-transduction using two-tone suppression
514 measurements." Sci Rep **9**(1): 4626.

515

516 ## Figure captions

517

518 **Figure 1. Sound-facilitated inner ear drug delivery**. Kainic acid was applied to the round window of young
519 gerbils under different acoustic conditions— in silence or with 60-75 dB SPL sounds. (**A**) Tuning curves at 30
520 dB SPL. The CFs of the three probing channels are 9.0, 3.8 and 1.8 kHz. (**B**) Normalized neural responses in
521 the AVCN versus the time of drug application. The drug effect time, t_E, was defined at the 75 percentiles of
522 normalized curves. In this measurement, it took 54 minutes to affect the 3.8 kHz CF location (green dashed
523 line and arrow). (**C**) DPOAEs were measured before and after the kainic acid delivery. Two stimulating tones
524 were at 40 dB SPL, and the frequency ratio was 1.1. The x-axis is the f_1 frequency. (**A-C**) Example of drug
525 delivered in silence ("Silence" case). (**D, E, F**) Example of drug delivery during the presentation of
526 broadband noise at 75 dB SPL ("Sound" case). (**G**) Response curves with colors representing CFs. Basal
527 (higher frequency) responses decay earlier. Out of 82 measurements, 48 silence-case curves are from 18
528 animals and 34 sound-case curves are from 13 animals. (**H**) Mean responses of sound and silence cases at
529 similar locations (CF = 4.5-6.5 kHz); n=19 for Silence, and n=13 for Sound. (**I**) Effect time versus CF location.
530 The shaded frequency range corresponds to the data in panel H. The broken curve ("Trend" line) was
531 obtained by fitting a curve to the silence data using 1D diffusion theory. (**J**) Effect time in dB with respect to
532 the trend line. t_E in dB = $20\log_{10}(t_E/t_{Trend})$. (**K**) Two-tailed t-tests between the effect times of sound and
533 silence cases for the entire CF range (whole, n=48, 34 for silence and sound), low-CF locations (<4.5 kHz,
534 n=24, 16 for silence and sound), and high-CF locations (> 4.5 kHz, n=24, 18 for silence and sound).
535 Throughout this paper, the symbols and range bars indicate the mean and the 95% confidence interval,
536 respectively.

537

538 **Figure 2. Suppressing motility of outer hair cells by salicylate**. Under the "post-SA" protocol, salicylic acid
539 (SA, 200 mg/kg) was administered IP before applying kainic acid at the round window. Broadband noise at
540 75 dB SPL was played during experiments. (**A**) DPOAEs before and after salicylic acid and kainic acid
541 delivery. (**B**) Overall response curves. IP salicylic acid was administered at t=0. The red vertical line indicates
542 when kainic acid was applied to the round window. The arrows indicate the application spans of salicylic
543 acid (SA) and kainic acid (KA). (**C**) Normalized neural responses after kainic-acid application (the curves after
544 the red line in panel B). (**D, E, F**) Another example of the post-SA protocol. (**G**) Effect time versus CF location
545 of post-SA measurements (n=22 from 8 animals). The silence-case trend line is the same as Fig. 1. (**H**) The
546 effect time in dB with respect to the trend line. (**I**) Two-tailed t-tests between the effect times of sound,
547 silence, and post-SA cases for the entire CF range (whole), low-CF locations (<4.5 kHz, n = 12 for the post-SA
548 case), and high-CF locations (> 4.5 kHz, n=10 for the post-SA case).

549

550 **Figure 3. Pure tones yield shorter effect times than broadband noise**. (**A**) Drug delivery during
551 presentation of a tone at low-frequency (0.5 kHz 80 dB SPL) or (**B**) mid-frequency (3.5 kHz 80 dB SPL). (**C**)
552 Effect time of drug delivery under the low- and mid-frequency tones. The trendline of the silence case is the
553 same as Fig. 1I. n = 18 from 6 animals for LF tone. n = 22 from 8 animals for MF tone. (**D**) Normalized effect
554 time. (**E**) Statistical comparison between the three cases (silence, low- and mid-frequency-tone protocols).
555 The two-tailed t-tests were performed on all CF locations, low-CF (< 4.5 kHz, n = 12, 9 for MF- and LF-tone)
556 and high-CF (> 4.5 kHz, n = 10, 8 for MF- and LF-tone) locations. (**F**) Normalized effect time under three
557 sound-conditions compared: Broadband noise, mid-frequency-tone and low-frequency-tone.

558

559 **Figure 4. Outer-hair-cell motility facilitates inner-ear drug delivery**. Summary of the effects of different
560 acoustic and physiological conditions on inner-ear drug delivery. The y-axes represent absolute effect time
561 in minutes (top) and relative effect time in dB w.r.t the trend line (bottom). The same trend line (broken
562 lines, obtained from the control case) is presented for all panels. (**A**, **B**) Effect time in silence. (**C**, **D**) Effect
563 time under 60 or 75 dB SPL broadband (0.1-12 kHz) sounds. (**E**, **F**) Effect time when outer-hair-cell motility
564 was suppressed by salicylate. Before kainic acid application, the salicylic acid solution was administered
565 systemically (intraperitoneally-IP, 200 mg/kg) or locally (round window-RW, 10 mM). (**G**, **H**) Effect time
566 under 80 dB SPL pure tones. A 0.5 kHz (low-frequency-LF) or 3-6 kHz (mid-frequency-MF) tone was
567 presented during drug delivery. The mid-frequency tone was chosen to match one of the probe
568 frequencies.

569

570 **Figure 5. Active outer hair cells drive fluid flow**. Inner-ear drug delivery was simulated using a
571 computational model. (**A**) Drug delivery due to diffusion. The concentration profile over the cochlear
572 length at 30 minutes after drug application to the round window. (**B**) Drug delivery with 80 dB SPL, 1-kHz
573 sound. The black contour line demonstrates how advection affects drug delivery. (**C**) Steady-state drift flow
574 of the cochlear fluids. Red and blue curves represent the clockwise and counterclockwise streamlines. (**D**)
575 The region with the fastest advection. The drift velocity (green color contour) is as large as a few mm/s.

Figures with Captions

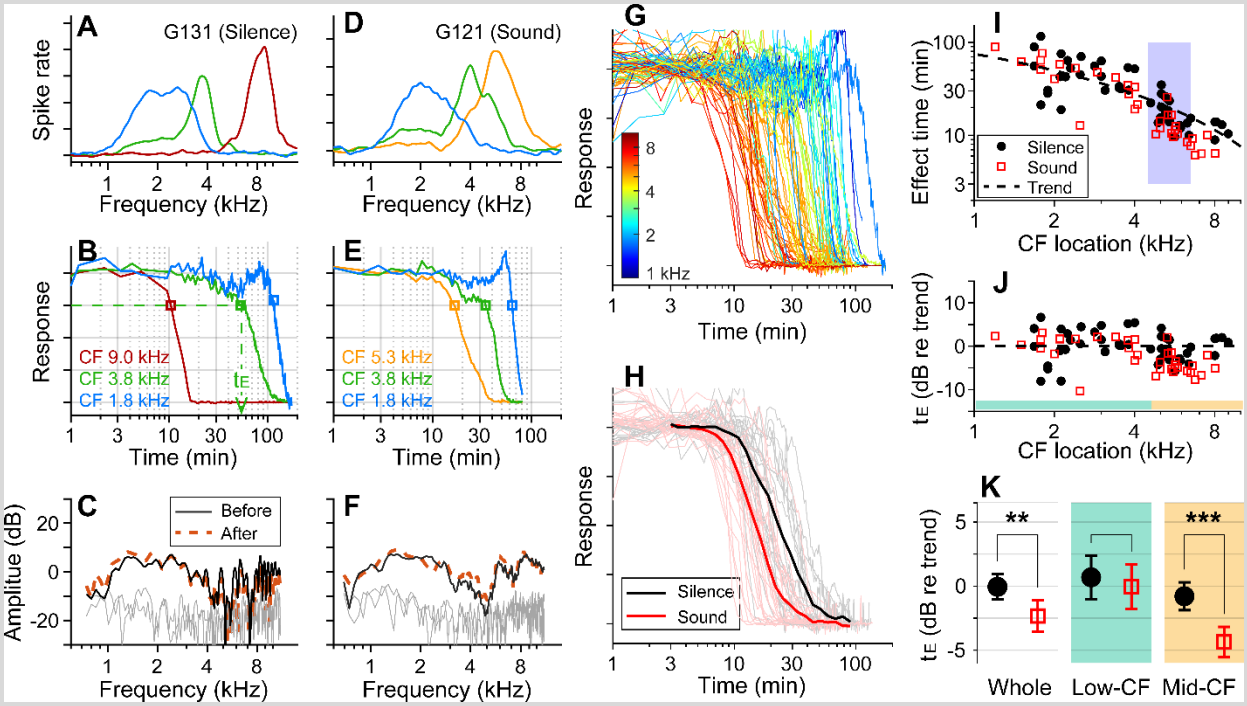

Figure 1. Sound-facilitated inner ear drug delivery. Kainic acid was applied to the round window of young gerbils under different acoustic conditions— in silence or with 60-75 dB SPL sounds. (**A**) Tuning curves at 30 dB SPL. The CFs of the three probing channels are 9.0, 3.8 and 1.8 kHz. (**B**) Normalized neural responses in the AVCN versus the time of drug application. The drug effect time, t_E, was defined at the 75 percentiles of normalized curves. In this measurement, it took 54 minutes to affect the 3.8 kHz CF location (green dashed line and arrow). (**C**) DPOAEs were measured before and after the kainic acid delivery. Two stimulating tones were at 40 dB SPL, and the frequency ratio was 1.1. The x-axis is the f_1 frequency. (**A-C**) Example of drug delivered in silence ("Silence" case). (**D, E, F**) Example of drug delivery during the presentation of broadband noise at 75 dB SPL ("Sound" case). (**G**) Response curves with colors representing CFs. Basal (higher frequency) responses decay earlier. Out of 82 measurements, 48 silence-case curves are from 18 animals and 34 sound-case curves are from 13 animals. (**H**) Mean responses of sound and silence cases at similar locations (CF = 4.5-6.5 kHz); n=19 for Silence, and n=13 for Sound. (**I**) Effect time versus CF location. The shaded frequency range corresponds to the data in panel H. The broken curve ("Trend" line) was obtained by fitting a curve to the silence data using 1D diffusion theory. (**J**) Effect time in dB with respect to the trend line. t_E in dB = $20\log_{10}(t_E/t_{Trend})$. (**K**) Two-tailed t-tests between the effect times of sound and silence cases for the entire CF range (whole, n=48, 34 for silence and sound), low-CF locations (<4.5 kHz, n=24, 16 for silence and sound), and high-CF locations (> 4.5 kHz, n=24, 18 for silence and sound). Throughout this paper, the symbols and range bars indicate the mean and the 95% confidence interval, respectively.

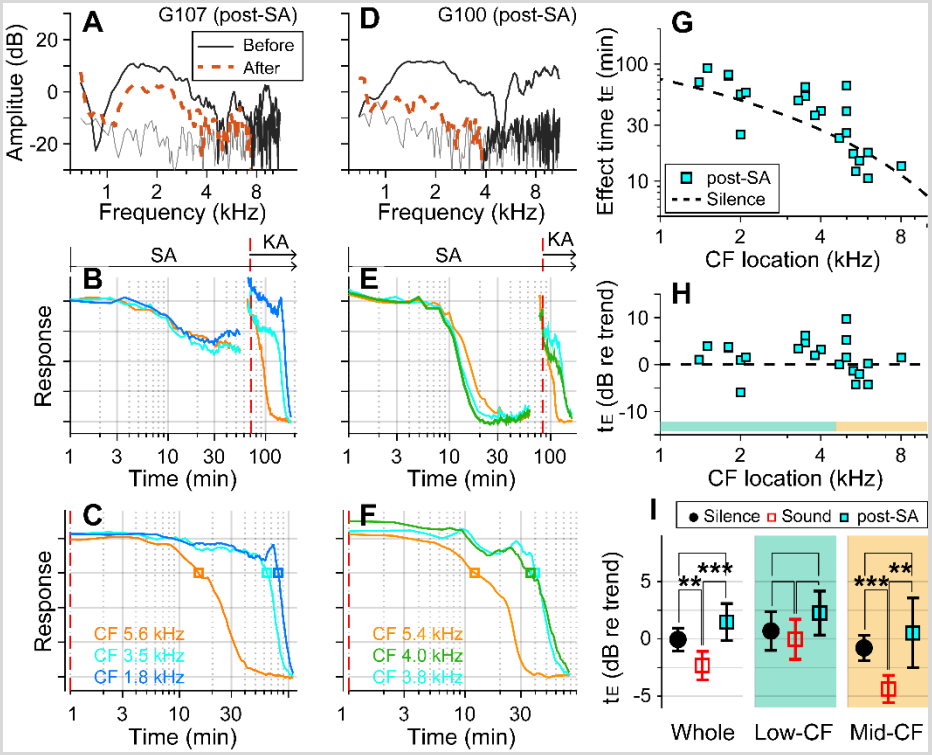

Figure 2. Suppressing motility of outer hair cells by salicylate. Under the "post-SA" protocol, salicylic acid (SA, 200 mg/kg) was administered IP before applying kainic acid at the round window. Broadband noise at 75 dB SPL was played during experiments. (**A**) DPOAEs before and after salicylic acid and kainic acid delivery. (**B**) Overall response curves. IP salicylic acid was administered at t=0. The red vertical line indicates when kainic acid was applied to the round window. The arrows indicate the application spans of salicylic acid (SA) and kainic acid (KA). (**C**) Normalized neural responses after kainic-acid application (the curves after the red line in panel B). (**D, E, F**) Another example of the post-SA protocol. (**G**) Effect time versus CF location of post-SA measurements (n=22 from 8 animals). The silence-case trend line is the same as Fig. 1. (**H**) The effect time in dB with respect to the trend line. (**I**) Two-tailed t-tests between the effect times of sound, silence, and post-SA cases for the entire CF range (whole), low-CF locations (<4.5 kHz, n = 12 for the post-SA case), and high-CF locations (> 4.5 kHz, n=10 for the post-SA case).

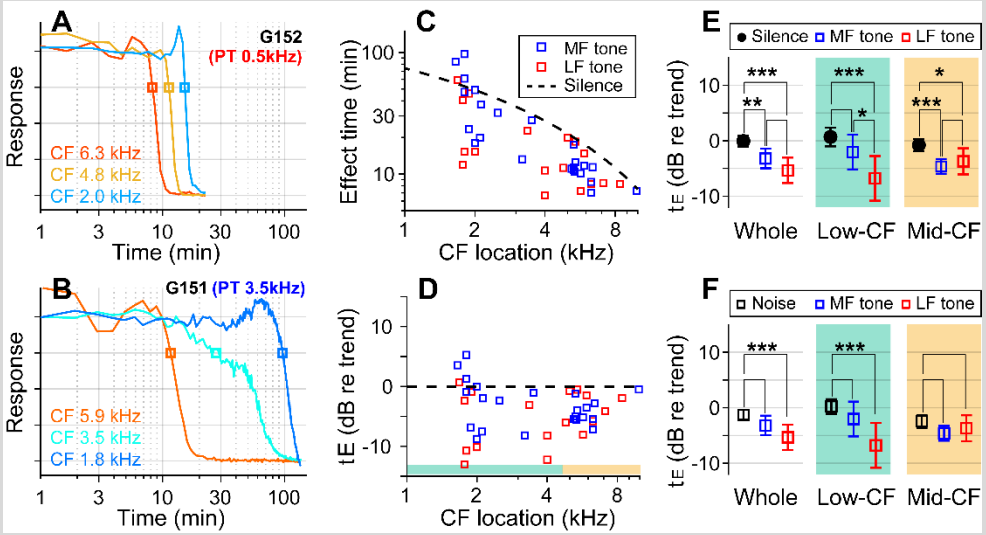

Figure 3. Pure tones yield shorter effect times than broadband noise. (**A**) Drug delivery during presentation of a tone at low-frequency (0.5 kHz 80 dB SPL) or (**B**) mid-frequency (3.5 kHz 80 dB SPL). (**C**) Effect time of drug delivery under the low- and mid-frequency tones. The trendline of the silence case is the same as Fig. 1I. n = 18 from 6 animals for LF tone. n = 22 from 8 animals for MF tone. (**D**) Normalized effect time. (**E**) Statistical comparison between the three cases (silence, low- and mid-frequency-tone protocols). The two-tailed t-tests were performed on all CF locations, low-CF (< 4.5 kHz, n = 12, 9 for MF- and LF-tone) and high-CF (> 4.5 kHz, n = 10, 8 for MF- and LF-tone) locations. (**F**) Normalized effect time under three sound-conditions compared: Broadband noise, mid-frequency-tone and low-frequency-tone.

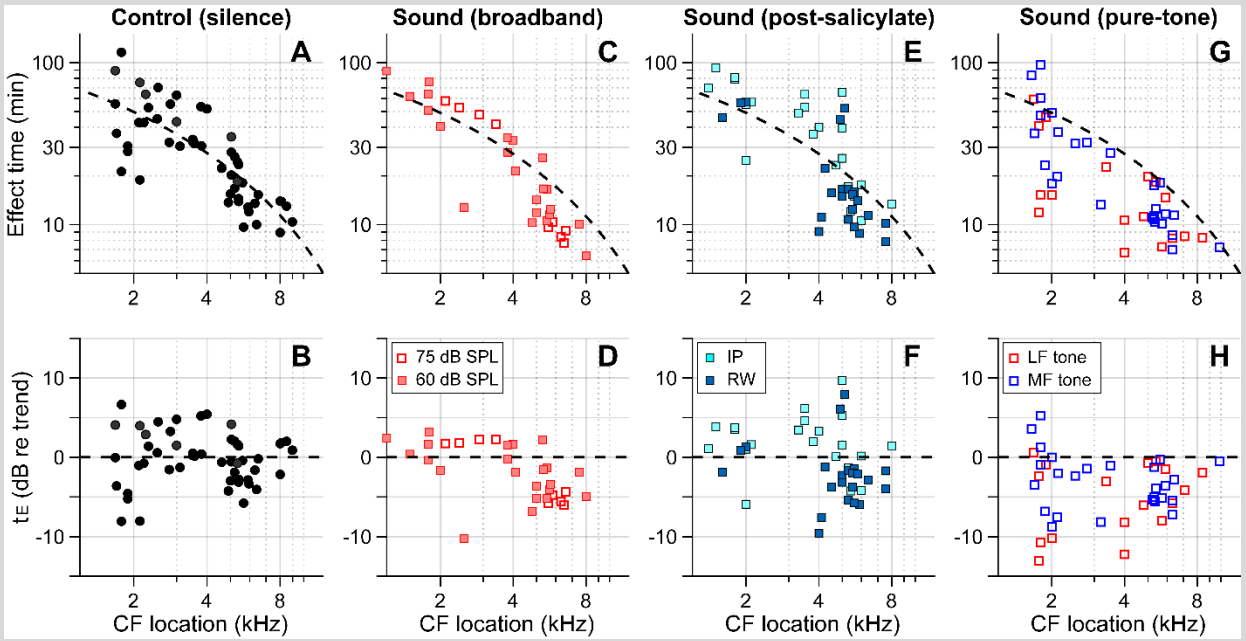

Figure 4. Outer-hair-cell motility facilitates inner-ear drug delivery. Summary of the effects of different acoustic and physiological conditions on inner-ear drug delivery. The y-axes represent absolute effect time in minutes (top) and relative effect time in dB w.r.t the trend line (bottom). The same trend line (broken lines, obtained from the control case) is presented for all panels. (**A**, **B**) Effect time in silence. (**C**, **D**) Effect time under 60 or 75 dB SPL broadband (0.1-12 kHz) sounds. (**E**, **F**) Effect time when outer-hair-cell motility was suppressed by salicylate. Before kainic acid application, the salicylic acid solution was administered systemically (intraperitoneally-IP, 200 mg/kg) or locally (round window-RW, 10 mM). (**G**, **H**) Effect time under 80 dB SPL pure tones. A 0.5 kHz (low-frequency-LF) or 3-6 kHz (mid-frequency-MF) tone was presented during drug delivery. The mid-frequency tone was chosen to match one of the probe frequencies.

584

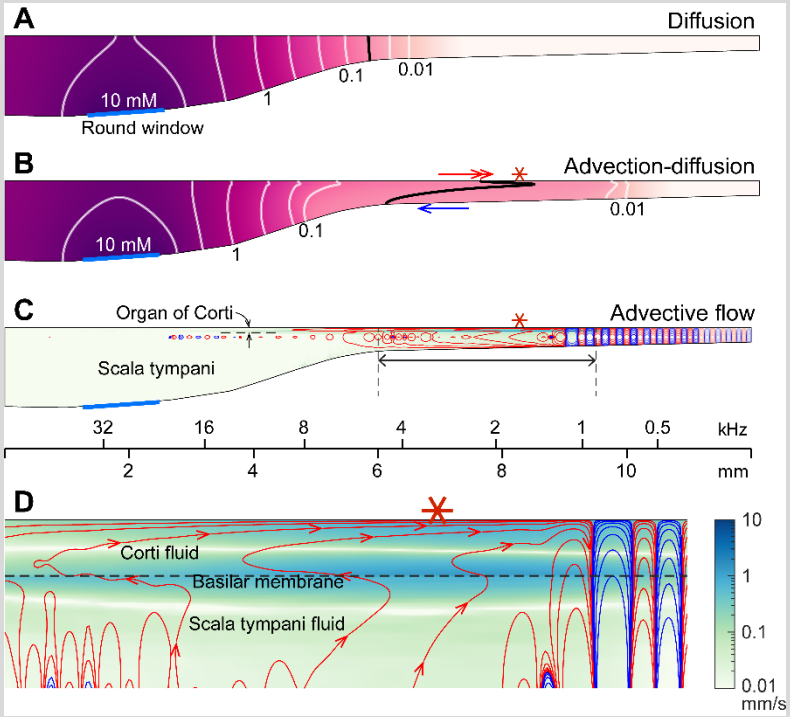

Figure 5. Active outer hair cells drive fluid flow. Inner-ear drug delivery was simulated using a computational model. (**A**) Drug delivery due to diffusion. The concentration profile over the cochlear length at 30 minutes after drug application to the round window. (**B**) Drug delivery with 80 dB SPL, 1-kHz sound. The black contour line demonstrates how advection affects drug delivery. (**C**) Steady-state drift flow of the cochlear fluids. Red and blue curves represent the clockwise and counterclockwise streamlines. (**D**) The region with the fastest advection. The drift velocity (green color contour) is as large as a few mm/s.

585

586

587

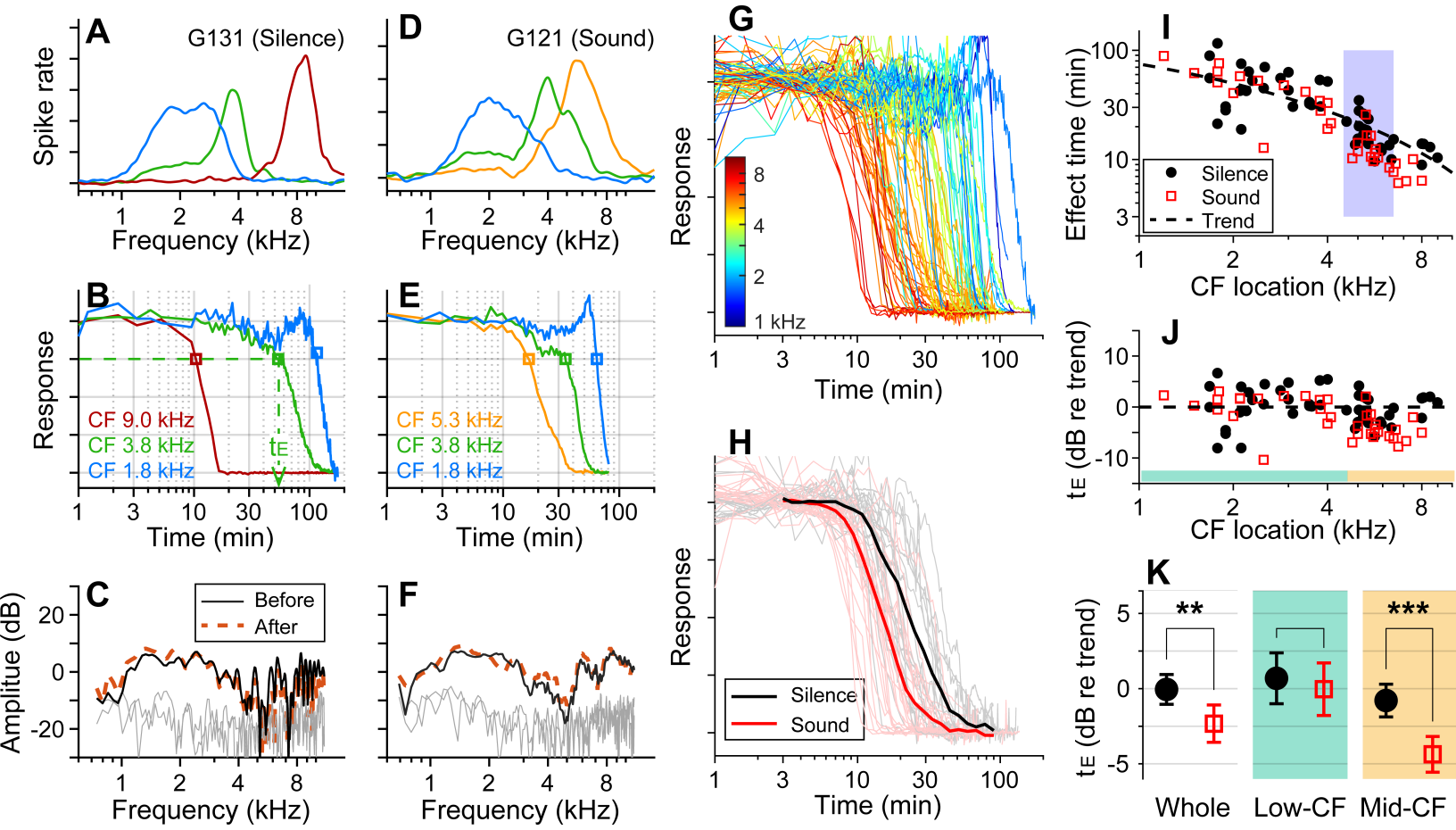
A
G131 (Silence)
Spike rate
Frequency (kHz)
D
G121 (Sound)
B
Response
CF 9.0 kHz
CF 3.8 kHz
CF 1.8 kHz
tE
Time (min)
E
CF 5.3 kHz
C
Before
After
Amplitue (dB)
F
G
8
4
2
1 kHz
H
Silence
Sound
I
Effect time (min)
CF location (kHz)
J
tE (dB re trend)
K
**
***
Whole
Low-CF
Mid-CF

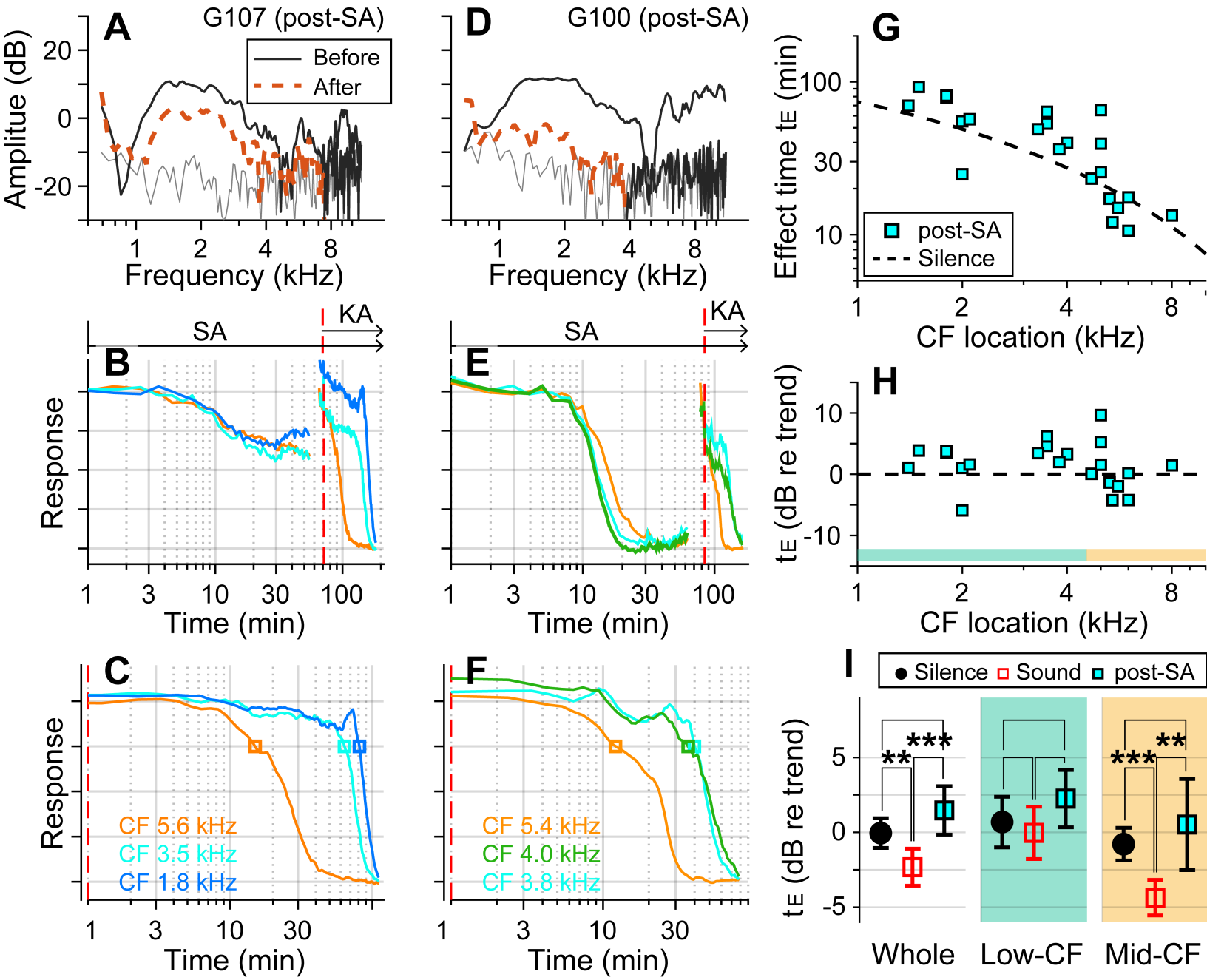
A
G107 (post-SA)
Before
After
Amplitue (dB)
20
0
-20
1
2
4
8
Frequency (kHz)
D
G100 (post-SA)
Frequency (kHz)
G
Effect time tE (min)
100
30
10
post-SA
Silence
CF location (kHz)
SA
KA
B
Response
1
3
10
30
100
Time (min)
E
H
tE (dB re trend)
10
0
-10
CF location (kHz)
C
CF 5.6 kHz
CF 3.5 kHz
CF 1.8 kHz
F
CF 5.4 kHz
CF 4.0 kHz
CF 3.8 kHz
I
Silence
Sound
post-SA
5
0
-5
**
***
Whole
Low-CF
Mid-CF

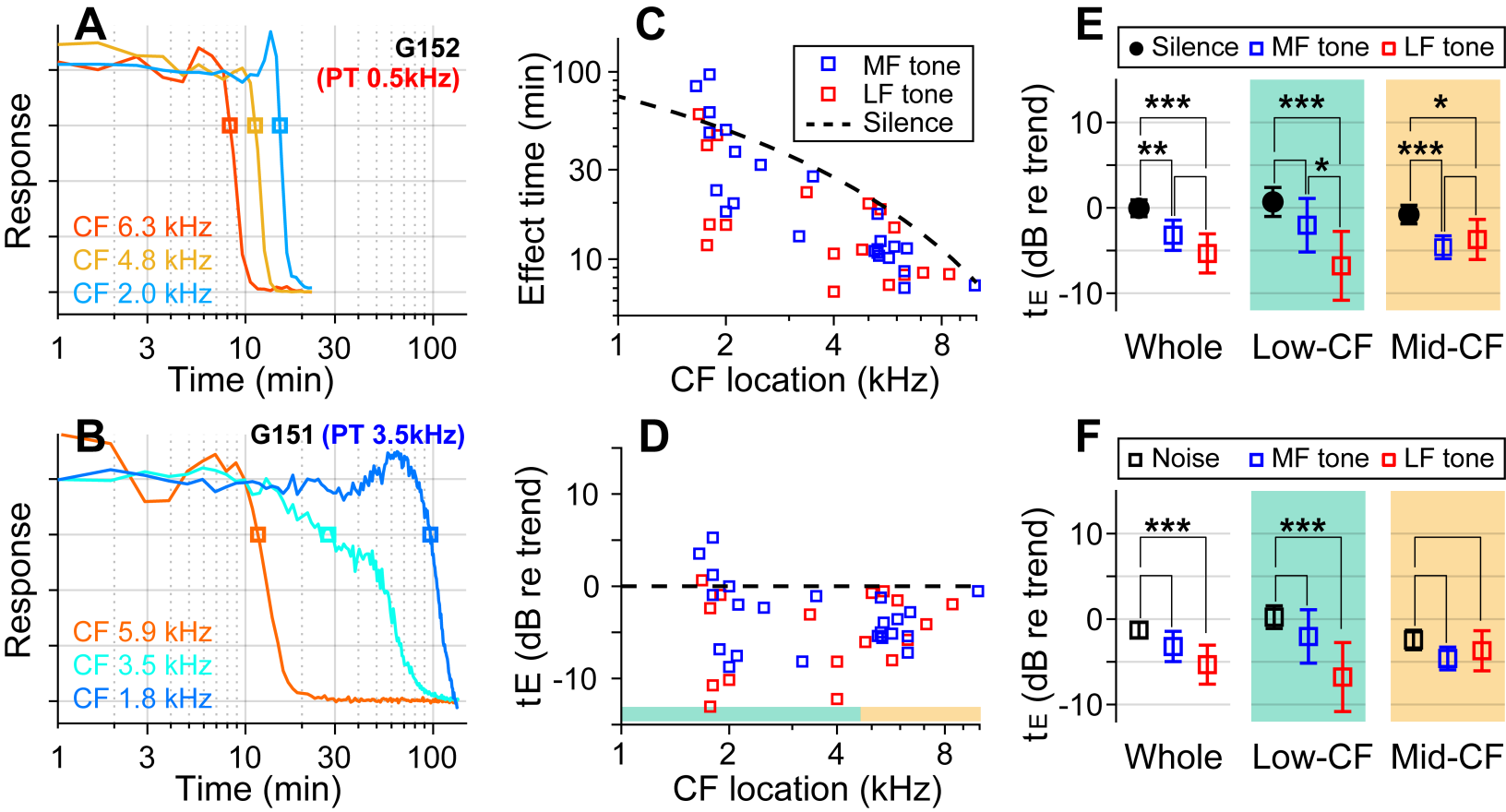
A
G152
(PT 0.5kHz)
Response
CF 6.3 kHz
CF 4.8 kHz
CF 2.0 kHz
1
3
10
30
100
Time (min)
B
G151 (PT 3.5kHz)
Response
CF 5.9 kHz
CF 3.5 kHz
CF 1.8 kHz
1
3
10
30
100
Time (min)
C
Effect time (min)
100
30
10
MF tone
LF tone
Silence
1
2
4
8
CF location (kHz)
D
tE (dB re trend)
10
0
-10
1
2
4
8
CF location (kHz)
E
Silence
MF tone
LF tone
tE (dB re trend)
10
0
-10
***
**
***
*
*
***
Whole
Low-CF
Mid-CF
F
Noise
MF tone
LF tone
tE (dB re trend)
10
0
-10
***
***
Whole
Low-CF
Mid-CF

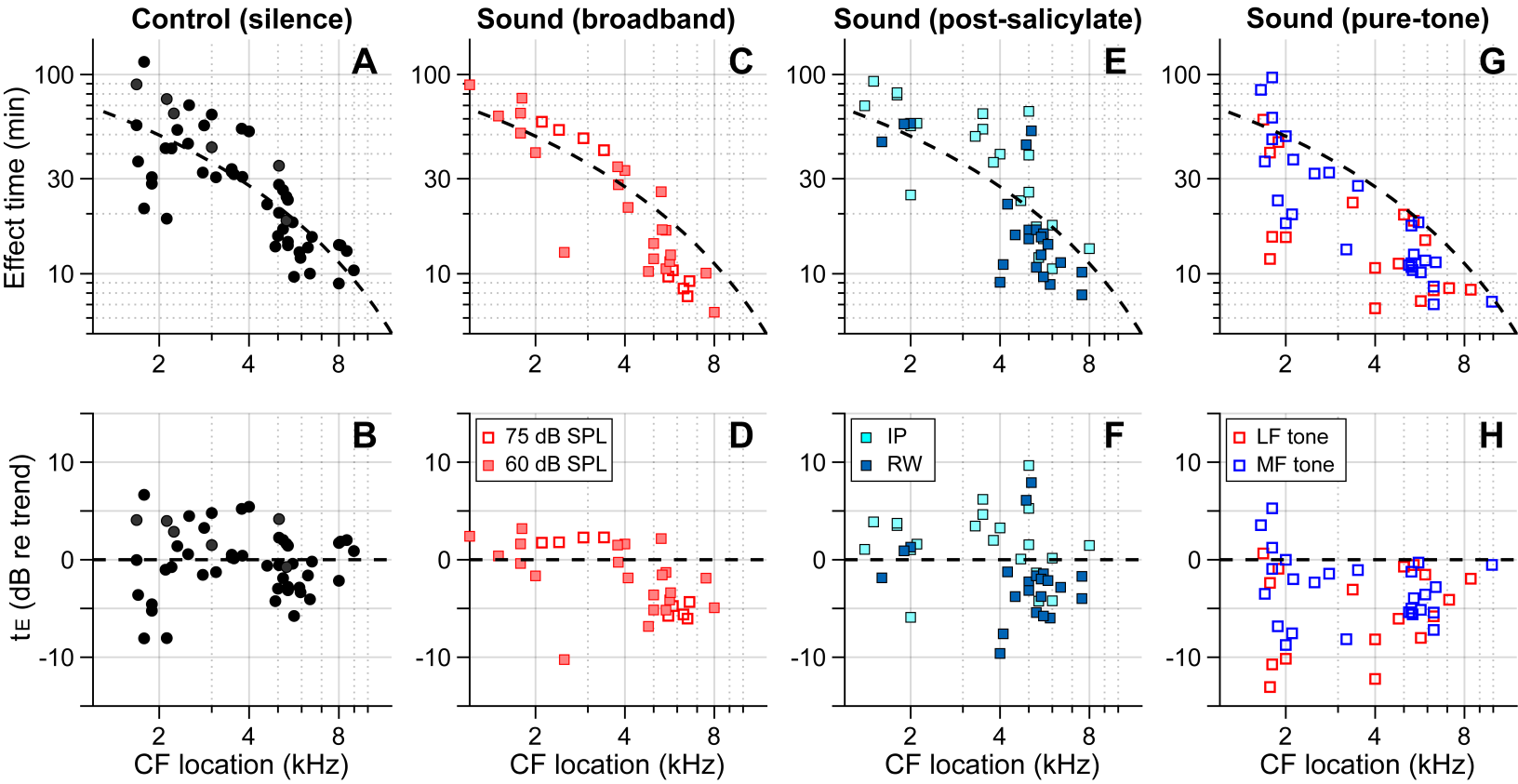
Control (silence)
Sound (broadband)
Sound (post-salicylate)
Sound (pure-tone)
A
B
C
D
E
F
G
H
Effect time (min)
tE (dB re trend)
CF location (kHz)
75 dB SPL
60 dB SPL
IP
RW
LF tone
MF tone

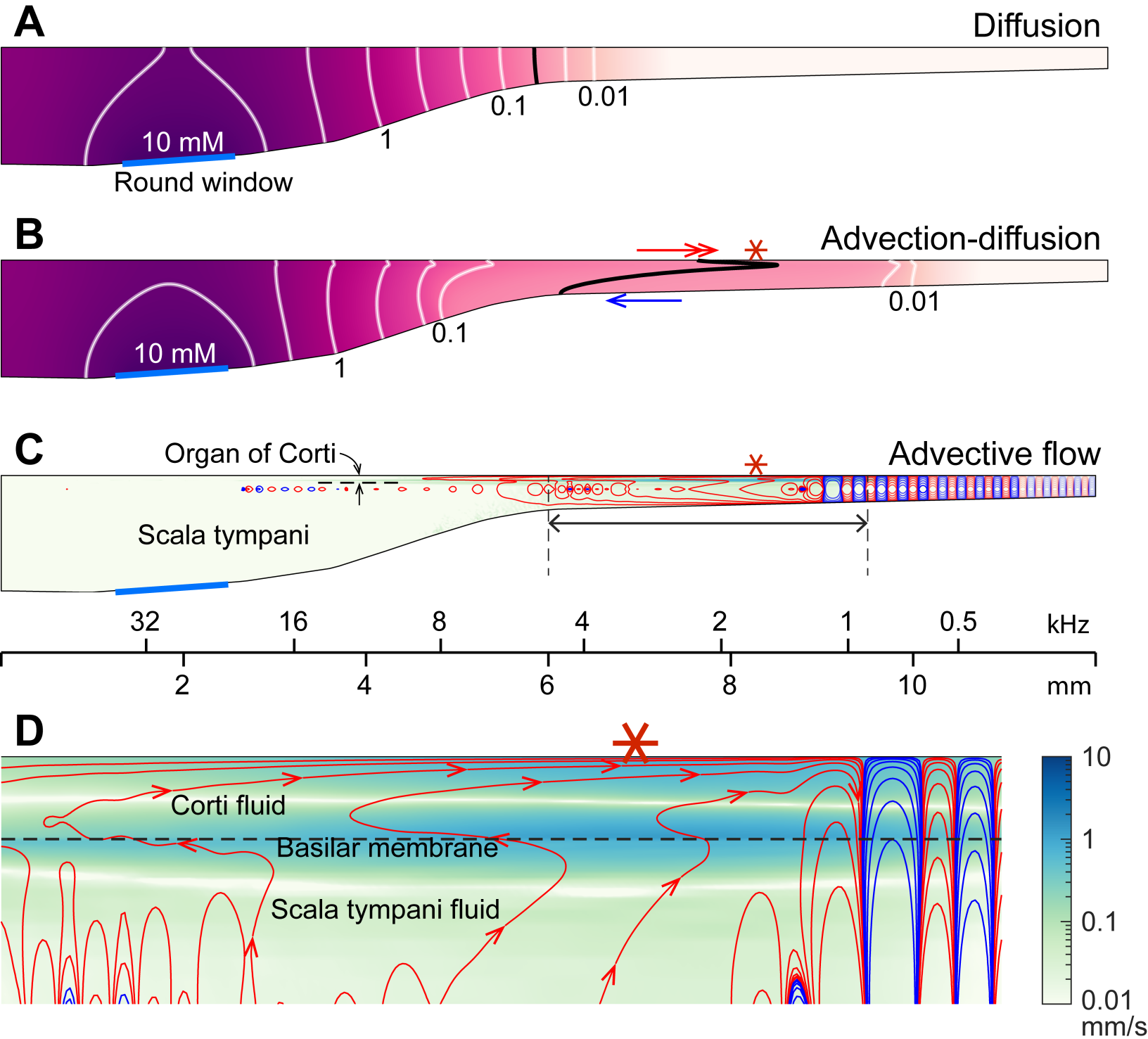
A
Diffusion
10 mM
Round window
1
0.1
0.01
B
Advection-diffusion
10 mM
1
0.1
0.01
C
Organ of Corti
Advective flow
Scala tympani
32
16
8
4
2
1
0.5
kHz
2
4
6
8
10
mm
D
Corti fluid
Basilar membrane
Scala tympani fluid
10
1
0.1
0.01
mm/s